Sign-Changing Photon-Mediated Atom Interactions in Multimode Cavity Quantum Electrodynamics

Yudan Guo, Ronen M. Kroeze, Varun D. Vaidya, Jonathan Keeling, and Benjamin L. Lev

Phys. Rev. Lett. **122**, 193601 — Published 14 May 2019

DOI: 10.1103/PhysRevLett.122.193601

Sign-changing photon-mediated atom interactions in multimode cavity QED

Yudan Guo,[1,2] Ronen M. Kroeze,[1,2] Varun D. Vaidya,[1,2,3] Jonathan Keeling,[4] and Benjamin L. Lev[1,2,3]

[1]*Department of Physics, Stanford University, Stanford, CA 94305*
[2]*E. L. Ginzton Laboratory, Stanford University, Stanford, CA 94305*
[3]*Department of Applied Physics, Stanford University, Stanford, CA 94305*
[4]*SUPA, School of Physics and Astronomy, University of St Andrews, St Andrews KY16 9SS UK*

(Dated: March 26, 2019)

Sign-changing interactions constitute a crucial ingredient in the creation of frustrated many-body systems such as spin glasses. We present here the demonstration of a photon-mediated sign-changing interaction between Bose-Einstein condensed (BEC) atoms in a confocal cavity. The interaction between two atoms is of an unusual, nonlocal form proportional to the cosine of the inner product of the atoms' position vectors. This interaction arises from the differing Gouy phase shifts of the cavity's degenerate modes. The interaction drives a nonequilibrium Dicke-type phase transition in the system leading to atomic checkerboard density-wave order. Because of the Gouy phase anomalies, the checkerboard pattern can assume either a sine or cosine-like character. This state is detected via the holographic imaging of the cavity's superradiant emission. Together with Ref. [1], we explore this interaction's influence on superradiant phase transitions in multimode cavities. Employing this interaction in cavity QED spin systems may enable the creation of artificial spin glasses and quantum neural networks.

The strong atom-photon interactions provided by cavity QED [2] open new avenues toward exploring quantum many-body physics in a nonequilibrium setting [3–5]. For example, cavity QED with Rydberg atoms provides strong nonlinear interactions between photons [6] and can lead to topologically nontrivial many-body states [7]. Nonequilibrium Dicke superradiant phase transitions [3, 5, 8] and other superradiant transitions [9, 10] have been observed in transversely pumped cavities with thermal atoms [11] and BECs [12, 13], including transitions leading to supersolids [14], superradiant Mott insulators [15, 16], and polariton condensates of supermode-density-waves [17] and spinors [18–20].

Superradiant phase transitions emerge for an ensemble of randomly distributed atoms trapped inside a transversely pumped cavity [9, 21]. Beyond a threshold pump strength, the cavity-photon-mediated interaction energy overcomes the kinetic energy cost associated with the formation of an atomic density wave (DW). Consequently, the atoms self-organize into a checkerboard pattern on the lattice formed by the transverse pump and cavity mode. The phases of the atomic DW and cavity mode are locked together and locked to either $\{0, \pi\}$ with respect to the pump, thus breaking a $\mathbb{Z}_2$ symmetry [9, 13, 22].

In the dispersive limit of cavity QED, where the pump field is not resonant with the cavity modes, the photon field may be adiabatically eliminated. These superradiant phase transitions may then be seen to arise from an effective Hamiltonian with an atom-atom interaction (or spin-spin interaction for spinful atoms) mediated by the exchange of virtually excited cavity photons [3, 19, 23]. Single-mode cavities support infinite-range interactions among the atoms, while multimode cavities provide the means for tuning the range of interactions [23] and may allow the formation of superfluid liquid crystalline-like states [24, 25]. Photon-mediated interactions might also be possible via the use of photonic waveguides [26] and are similar to the phonon-mediated interactions demonstrated among trapped ions [27–29].

While tunable in range, the interactions among neutral atoms i, j have been demonstrated with only a fixed-sign coupling J_{ij} [23]. A wider range of many-body phenomena might be possible if J_{ij} were to flip in sign, because sign-flipping can induce frustrated interactions, as has been demonstrated with ions [30]. With the addition of positional randomness, structural [24, 25] and spin glasses [31, 32] of atoms in multimode cavities and waveguides [33] may be possible. These fascinating states exhibit rigidity that arises from a complex—and in some limits, unknown—order and symmetry breaking [34, 35]. Creating a tunable-interaction-range spin glass in the quantum-optical setting would provide a novel platform for investigating both how such order emerges, and how quantum phenomena may affect glassy physics.

In a step toward this goal, we demonstrate a sign-changing, nonlocal J_{ij} using a multimode cavity. Previously, we presented a derivation of this term and provided experimental evidence for its existence [23]. However, the work neither demonstrated its sign-changing property, nor explored an additional DW degree of freedom that arises due to the Gouy phase anomalies. This degree of freedom corresponds to a BEC in a multimode cavity adopting a DW pattern of either $\cos k_r z$ or $\sin k_r z$ character (along the cavity axis $\hat{z}$). Here, $z = 0$ is defined at the cavity center, $k_r = 2\pi/\lambda$, and $\lambda = 780$ nm is the cavity and pump wavelength. We discuss the nonlocal term and how this new DW degree of freedom can be tuned before presenting results of three experiments. The first and second experiments demonstrate the switching between $\cos k_r z$ or $\sin k_r z$ DWs for a cavity with one

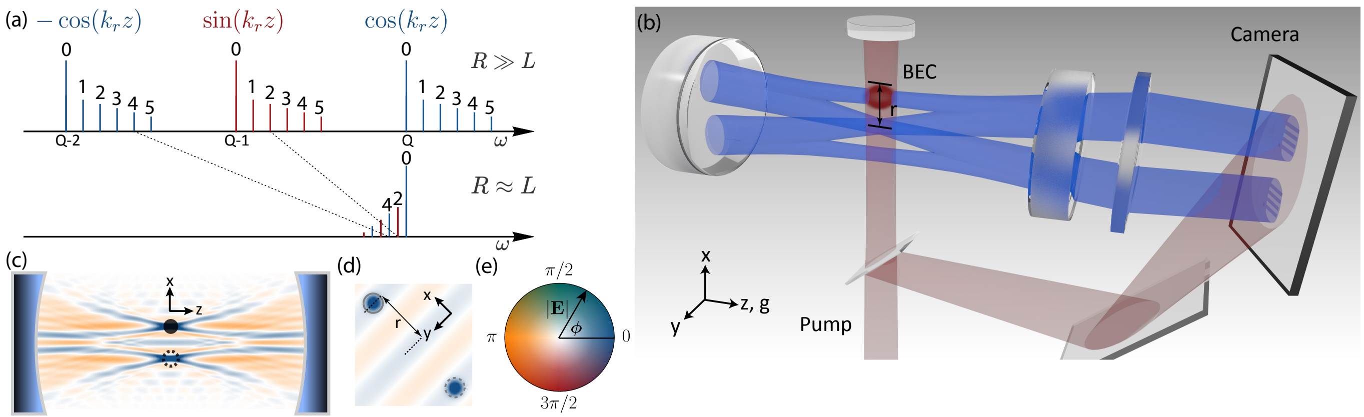

FIG. 1. (a) Relationship between modes in a near-planar cavity (upper) versus a near-confocal cavity (lower). As $R \to L$, higher-order transverse modes shift further in frequency than lower-order modes due to differential Gouy phases. (Near-)degenerate resonances arise at confocality ($R \approx L$) comprised of modes (either even or odd) from different longitudinal families Q with different longitudinal patterns, as indicated. (b) Sketch of experimental apparatus showing one of two possible BECs (red sphere) confined within the cavity by optical tweezer traps (not shown). Two images (real and mirror) of the supermode created by the BEC appear in the cavity emission due the fixed parity of the confocal cavity modes [17, 23, 36]. Spatial heterodyning of the emitted field is performed by interfering the pump laser (red) and cavity emission (blue) at the EMCCD camera. (b,c) Simulation illustrating (d) the intracavity field pattern and (e) resulting camera image of the object plane. Simulated camera image shows two bright spots (emitted from the BEC position and its mirror image) and an oscillating emission pattern between them. In a ray-tracing picture, the mode of a confocal cavity adopts a bow tie pattern [36]; in the wave picture shown here, spots emerge from the bow tie's arms, and an interference pattern from the bow tie's cross. U_{nonlocal} arises from photons exchanged via this interference field, hence its oscillatory form, while photons exchanged via the bright spots induce the U^{+}_{local} terms. (e) Color wheel illustrating the complex electric field.

and two intracavity BECs, resp., while the third demonstrates the sign-changing capability of the interaction using two intracavity BECs moved relative to one another. A companion paper [1] presents background theory and corroborating experiments in addition to other aspects of interactions induced by Gouy phase anomalies.

The nonlocal interaction term U_{nonlocal} arises from the differing Gouy phase shifts of the degenerate modes of the near-confocal multimode cavity. Gouy phase anomalies occur in any focused wave and lead to a phase advance as the field propagates through its waist [36–41]. Fields of higher-order Hermite-Gaussian transverse profiles $\Xi_{l,m}$ exhibit Gouy phase shifts that increase as $1 + l + m$. This causes transverse $\text{TEM}_{l,m}$ modes of a cavity with the same longitudinal mode number Q to resonate at different frequencies. However, when special geometrical conditions are met, as, e.g., in a confocal cavity, transverse modes with differing Q become degenerate; see Fig. 1(a). At one such degenerate frequency, all modes are either even- or odd-parity. We employ an even-parity resonance, and therefore, mirror images of the same field amplitude are supported symmetrically across the cavity axis. See Fig. 1(c).

The differing Gouy phases of the modes affect the form of the interaction because the photon-mediated interaction in a multimode cavity arises from the exchange of photons in a superposition of all available modes at the positions of the two atoms [23–25]. When accounted for in the sum over all modes, the Gouy phases contribute an additional interaction energy U_{nonlocal} to the local interaction; Ref. [1] provides a more physically intuitive description of the origin of this effect. The form of the nonlocal term is derived in Refs. [1, 23] to be $U_{\text{nonlocal}}(\mathbf{r}_i, \mathbf{r}_j) = J_0 \mathcal{D}_{\text{nonlocal}}(\mathbf{r}_i, \mathbf{r}_j) \cos k_r x_i \cos k_r x_j$, where $\mathbf{r}_i$ are (x, y) coordinates of atom i, $\mathcal{D}_{\text{nonlocal}}(\mathbf{r}_i, \mathbf{r}_j) = \cos(2\mathbf{r}_i \cdot \mathbf{r}_j / w_0^2)/4\pi$, and $w_0 = 35$ μm is the $\text{TEM}_{0,0}$ mode waist. The coupling strength is $J_0 = g_0^2 \Omega^2 / \Delta_a^2 \Delta_{0,0}$, where $g_0 = 2\pi \times 1.47(3)$ MHz is the vacuum Rabi rate for an atom coupled to the center of the $\text{TEM}_{0,0}$ mode, Ω^2 is proportional to the pump intensity, and $\Delta_a = -2\pi \times 102$ GHz is the detuning of the pump from the atomic excited state. The position-dependent prefactors $\cos k_r x_i$ appearing in the interaction arise due to the standing-wave pump [42]. The local interaction is comprised of the real and mirror image terms $U^{\pm}_{\text{local}}(\mathbf{r}_i, \mathbf{r}_j) = U_{\text{local}}(\mathbf{r}_i, \mathbf{r}_j) \pm U_{\text{local}}(\mathbf{r}_i, -\mathbf{r}_j)$ [1, 23], where $\pm$ correspond to even (odd) resonances; we employ even.

In addition to U_{nonlocal}, the Gouy phases induce a division of the cavity resonances into two classes with alternating out-of-phase longitudinal DW patterns, either $\sin(k_r z + \delta)$ or $\cos(k_r z + \delta)$, where $\delta = \{0, \pi\}$; see Fig. 1(a). At an even-mode confocal cavity resonance, the total mode function is $\Phi_{Q,l,m}(x, y, z) \propto \Xi_{l,m}(x, y) \cos(k_r z + \delta)$ for $l + m \bmod 4 = 0$ modes, while $\Phi_{Q,l,m}(x, y, z) \propto \Xi_{l,m}(x, y) \sin(k_r z + \delta)$ for $l +$

m mod $4 = 2$ modes [43]. Thus, while in a single-mode cavity $H \propto J_0 \cos k_r z_i \cos k_r z_j$, in a confocal cavity, the total interaction is

$$U \propto U_c(\mathbf{r}_i, \mathbf{r}_j) \cos k_r z_i \cos k_r z_j + U_s(\mathbf{r}_i, \mathbf{r}_j) \sin k_r z_i \sin k_r z_j,$$

where $U_{c,s} = U^{+}_{\text{local}} \pm U_{\text{nonlocal}}$ [1, 23]. Moreover, while the atomic wavefunction may be expanded as $\Psi = \psi_0 + \sqrt{2}\psi_c \cos k_r x \cos k_r z$ in a single-mode cavity, an additional atomic field is required in a confocal cavity: $\Psi = \psi_0 + \sqrt{2} \cos k_r x[\psi_c \cos k_r z + \psi_s \sin k_r z]$. Here, $\psi_{c,s}$ are the wavefunctions describing the fraction of atoms organized into the orthogonal sine versus cosine quadratures of the longitudinal profile; ψ_0 is the initial BEC wavefunction in the optical dipole trap [44]. The BEC condenses into either the sine or cosine DW according to which DW minimizes energy at the BEC position. We note that this choice of DW is solely determined through U_{nonlocal} since the $U_{c,s}$ have the same contribution from U^{+}_{local}. The remaining $\mathbb{Z}_2$ symmetry of the checkerboard pattern (i.e., the choice of $\delta = \{0, \pi\}$) is spontaneously broken as in a single-mode cavity.

The order parameter associated with the transition is composed of the fractions of atoms acquiring a λ-periodic density modulation in either of the two DWs patterns and the δ phase of the wave therein; in terms of these wavefunctions, the order parameters are $\chi_{c,s} = \psi_0\psi_{c,s}/N$, where N is the BEC population. Each χ may be viewed as a pseudospin with max/min value ± 1; the sign of χ indicates the relative pseudospin alignment. For BECs at $\mathbf{r}_i$ and $\mathbf{r}_j$, one may transform the system's light-matter interaction into an effective spin interaction Hamiltonian of the form $H_{ij} = -J_{ij}(\chi_{ci}\chi_{cj} - \chi_{si}\chi_{sj})$ after spatial integration [45]. Here, $J_{ij} \propto N J_0 \mathcal{D}_{\text{nonlocal}}(\mathbf{r}_i, \mathbf{r}_j)$ and N is each BEC's population. The total effective single-BEC Hamiltonian interaction is $H_1 = H_{ii}$. The BEC organizes into χ_c or χ_s depending on which DW pattern minimizes H_{ii}, i.e., whether J_{ii} is positive or negative. Likewise, for two BECs of equal size and shape, $H_2 = H_{ii} + H_{jj} + 2H_{ij}$.

The experimental apparatus is shown in Fig. 1(c). The BECs contain $\sim 2\times 10^5$ ^{87}Rb atoms in the $|F = 1, m_F = -1\rangle$ state. Optical tweezers position and confine each BEC in a tight trap of diameter <10 μm—smaller than w_0. See Refs. [23, 45, 46] for BEC preparation and optical tweezing procedures. To measure the field amplitude and phase of the superradiant emission, the cavity field and part of the pump are interfered on an EMCCD camera. This spatial heterodyne measurement is holographically reconstructed to provide the cavity field amplitude and phase; see Fig. 1(c-f) and Refs. [19, 47].

Cavity field-emission measurements may be interpreted as cavity-enhanced Bragg scattering: in the organized phase, the transverse pump light is Bragg scattered into the cavity mode from the atomic checkerboard pattern. The phase of the coherently scattered light is therefore directly correlated with the phase of the DW. In addition, in a near-confocal cavity, organization into

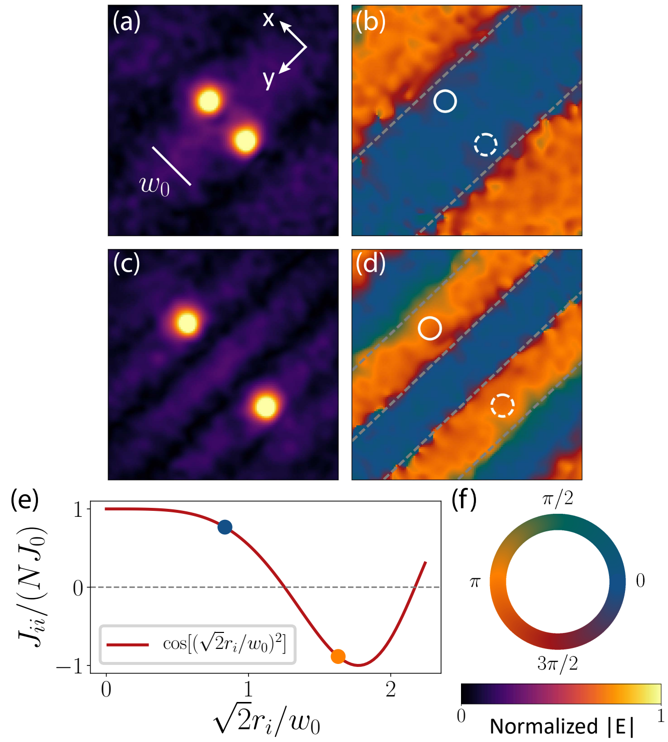

FIG. 2. (a–d) Extracted superradiant field at the two different positions marked in (e). (a,c) Plots of the extracted normalized field amplitude. (b,d) Plots of the corresponding phase data. The dotted lines mark the location of the nodes in the cosine pattern as determined from a functional fit to U_{nonlocal}. The phase of the electric field flips by π (while the periodicity shortens) as the BEC's position $\mathbf{r}$ is moved across a node in the cosine pattern. The length scale in panels (a–d) is indicated by the white line in panel (a) showing the cavity waist w_0. (e) Plot of the functional form of J_{ii}. The blue and orange dots mark the position of the BEC for the superradiant emission images above. The observed phase change is consistent with the flipped sign of J_{ii}. (f) Color scale for extracted phase and electric field amplitude, where the phase at $r = 0$ is set to 0.

χ_c (χ_s) is heralded by a 0 (π) phase shift between the cavity emission from the position of the BEC and its mirror image (due to U_{local}) versus that from the center of cavity (due solely to U_{nonlocal}) [1]. This phase shift may be traced back to the $\pm$-sign difference between the U_{local} and U_{nonlocal} terms in $U_{c,s}$ [1]. Figure 2 presents observations of this effect, where the amplitude and phase of superradiant emission from a single BEC at two different positions $\mathbf{r}_i$ is shown. These data demonstrate the ability to tune the DW order from a cosine to sine pattern by controlling $\mathbf{r}_i$ [48].

Measurements of $\chi_{c,s}$ are possible using two intracavity BECs. Absent cross-coupling, each BEC can independently choose a δ phase of its DW pattern, resulting in an enlarged $\mathbb{Z}_2 \otimes \mathbb{Z}_2$ symmetry for the system. Detection of their relative checkerboard states is possible

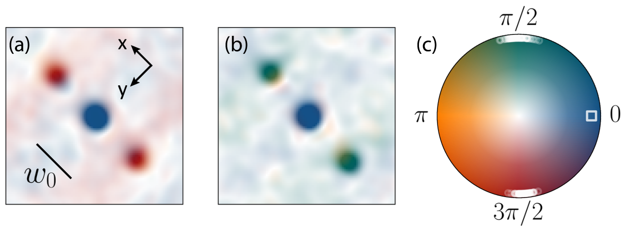

FIG. 3. (a,b) The measured electric field for two different realizations of the experiment. The $\pm\pi/2$ phase difference between the two BECs indicates that the BEC at $r = 0$ is in a cosine DW, while the other is in a sine wave DW. The sign-flips are indicative of the relative choice of phase δ due to $\mathbb{Z}_2$-symmetry-breaking in each DW. (c) Color disk for the plotted electric field. The white circular markers register the phase difference between the two spots in 186 shots of the experiments. We measured 92 shots of $\pi/2$ and 94 shots $3\pi/2$. The square marker indicates the reference phase of the $r = 0$ BEC: the phase of the light at $r = 0$ is set to 0 since we choose cosine DWs to scatter light with 0 relative phase.

since a χ_c DW is $\pm\pi/2$ out of phase from a χ_s DW, where the $\pm$-sign reflects the relative δ-phase of their checkerboard states. That is, the $\text{sgn}\{\chi_{c,s}\} = +1$ DW is $\delta = \pi$ out of phase from the $\text{sgn}\{\chi_{c,s}\} = -1$ DW. To observe this effect, we place one BEC at $r_1 = 0$ and the other at $r_2 = \sqrt{\pi}w_0/\sqrt{2}$, as shown in Fig. 3a. This sets $J_{11} = -J_{22} = N$ and the cross-term $H_{12} = 0$ because the J_{ii} terms cause the two BECs to prefer opposite DW quadratures (sine versus cosine). That is, the cross-terms in H_{12} vanish $\chi_{c1}\chi_{c2} = \chi_{s1}\chi_{s2} = 0$ since $\chi_{c1} \neq 0$ & $\chi_{s1} = 0$ for the first BEC and $\chi_{c2} = 0$ & $\chi_{s2} \neq 0$ for the second. This is shown in the measured electric fields of Fig. 3(b,c). We see that the phase of light emitted at the $r \neq 0$ BEC (along with the bow tie interference fringe at which it is located) is indeed shifted by $\pm\pi/2$. Because each BEC is free to choose between the $\mathbb{Z}_2$-symmetric checkerboard states within the preferred DW profile, we observe a random, nearly 50/50 distribution in relative sign over the course of multiple experimental realizations. This lack of $\mathbb{Z}_2$-broken-symmetry bias indicates the absence of inter-BEC coupling (i.e., $H_{12} = 0$), as intended [49].

Having demonstrated the DW-pattern-shifting effect of U_{nonlocal}, we now present observations of its sign-changing character. Again, we use two BECs, but fix one BEC at $r_1 = \sqrt{2\pi}w_0$, which sets $J_{11} = N$, while moving the position r_2 of the second BEC in a range of positions satisfying $J_{22} > 0$; see Fig. 4. This causes each BEC to energetically prefer organization into the same DW pattern, $\cos(k_r z + \delta)$, associated with pseudospins χ_{c1} and χ_{c2}, but leaves each DW's δ (i.e., its checkerboard pattern) free to be determined through the nonlocal cross-term interaction J_{12}. The relative pseudospin alignment of χ_{c1} versus χ_{c2} is then set by each DW's choice of δ. The coupling of the DWs via H_{12} locks the BECs' DW patterns to each other, reducing the symmetry to a single $\mathbb{Z}_2$, as in the single BEC case. J_{12} is positive in the region between $r_2 = 0$ and $r_2 \approx \sqrt{2\pi}w_0/4$, and so the two pseudospins align such that $\text{sgn}\{\chi_{c1}\chi_{c2}\} = +1$. However, as the cross-term interaction strength approaches 0 near $r_2 \approx \sqrt{2\pi}w_0/4$, the relative phase between the DWs becomes uncorrelated and randomly fluctuates between 0 and π, reflecting the re-emergence of the $\mathbb{Z}_2 \otimes \mathbb{Z}_2$ symmetry. This can be seen by comparing the plot of J_{12} in Fig. 4e with the data. For larger r_2's, J_{12} changes sign, causing an antiferromagnetic alignment $\text{sgn}\{\chi_{c1}\chi_{c2}\} = -1$ and reduction down to a single $\mathbb{Z}_2$ again. This is manifest in a π relative phase change between the light emitted from the two BECs [50]. To track this interaction sign change, we measure the field phase at each r_2 and plot the phase difference between the two sets of spots in Fig. 4e.

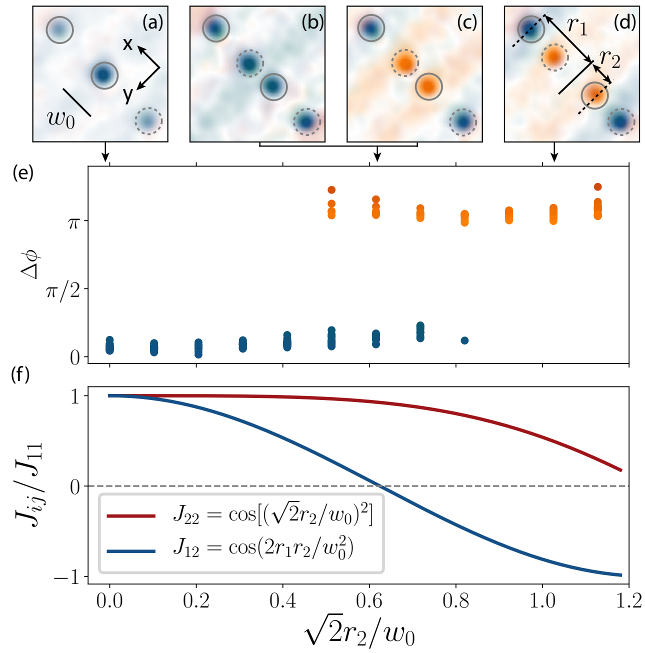

FIG. 4. (a–d) Examples of measured fields versus r_2 for two BECs on either side of the cavity center. r_1 of the first BEC is set so that $J_{11}/N = 1$. Panels (b,c) taken at the r_2 where $J_{12} = 0$. Random π phase flips are observed at this position and in the vicinity of small J_{12} with width primarily set by BEC size and the ramp rate of the pump. (e) Phase difference between the BECs' spots versus r_2. Twenty data points are plotted for each r_2. (f) Calculation of the self-interaction J_{22} and cross-interaction J_{12} versus r_2. Positive J_{22} (and J_{11}) ensures that $\cos k_r z$ is energetically favorable for both BECs until the sign flip in J_{12} causes the second BEC to condense into opposite pseudospin alignment with $\text{sgn}\{\chi_{c1}\chi_{c2}\} = -1$. See Fig. 3d for color disk scheme. Similar to Fig. 3, the phase of the light at r_1 is set to 0.

We have demonstrated that the nonlocal interaction arising from Gouy phase anomalies in a confocal cavity offers a new tool to engineer cavity-mediated atom-atom interactions. Freezing the atoms into position, e.g., with an optical lattice, and coupling the atomic spins as in Ref. [19], would allow U_{nonlocal} to mediate sign-changing spin-spin interactions of the form $\cos(2\mathbf{r}\cdot\mathbf{r}'/w_0^2)$. This demonstration of sign-changing photon-mediated interactions, in conjunction with our recent demonstrations of spin-spin interactions [19] and tunable-range atom-atom interactions [23]—all within the same experimental apparatus—open the door to creating artificial spin glasses. With optical tweezers to place atoms in reproducible configurations [51, 52], the exploration of replica symmetry breaking might be possible [34]. While replica symmetry breaking should be manifest in infinite-range spin glasses, the microscopic state of short-range spin glasses remains an outstanding question in statistical mechanics [35]. Moreover, placing atoms in specific locations to realize a particular graph of $\pm J_{ij}$ connectivity may provide a means for performing combinatorial optimization and Hopfield associative memory [31, 53–55] in a quantum-optical setting.

We acknowledge funding support from the Army Research Office, the National Science Foundation under Grant No. CCF-1640075, and the Semiconductor Research Corporation under Grant No. 2016-EP-2693-C. J. K. acknowledges support from SU2P.

[1] Y. Guo, V. D. Vaidya, R. M. Kroeze, R. A. Lunney, B. L. Lev, and J. Keeling, "Emergent and broken symmetries of atomic self-organization arising from Gouy phases in multimode cavity QED," (2018), arXiv:1810.xxxx.

[2] H. J. Kimble, "Strong Interactions of Single Atoms and Photons in Cavity QED," Phys. Scr. **T76**, 127 (1998).

[3] H. Ritsch, P. Domokos, F. Brennecke, and T. Esslinger, "Cold atoms in cavity-generated dynamical optical potentials," Rev. Mod. Phys. **85**, 553 (2013).

[4] L. M. Sieberer, M. Buchhold, and S. Diehl, "Keldysh field theory for driven open quantum systems," Rep. Prog. Phys. **79**, 096001 (2016).

[5] P. Kirton, M. M. Roses, J. Keeling, and E. G. Dalla Torre, "Introduction to the Dicke Model: From Equilibrium to Nonequilibrium, and Vice Versa," Advanced Quantum Technologies , 1800043 (2018).

[6] T. Peyronel, O. Firstenberg, Q.-Y. Liang, S. Hofferberth, A. V. Gorshkov, T. Pohl, M. D. Lukin, and V. Vuletić, "Quantum nonlinear optics with single photons enabled by strongly interacting atoms," Nature **488**, 57 (2012).

[7] N. Schine, A. Ryou, A. Gromov, A. Sommer, and J. Simon, "Synthetic Landau levels for photons," Nature **534**, 671 (2016).

[8] F. Dimer, B. Estienne, A. S. Parkins, and H. J. Carmichael, "Proposed realization of the Dicke-model quantum phase transition in an optical cavity QED system," Phys. Rev. A **75**, 013804 (2007).

[9] A. T. Black, H. W. Chan, and V. Vuletiç, "Observation of Collective Friction Forces due to Spatial Self-Organization of Atoms: From Rayleigh to Bragg Scattering," Phys. Rev. Lett. **91**, 203001 (2003).

[10] J. G. Bohnet, Z. Chen, J. M. Weiner, D. Meiser, M. J. Holland, and J. K. Thompson, "A steady-state superradiant laser with less than one intracavity photon," Nature **484**, 78 (2012).

[11] Z. Zhiqiang, C. H. Lee, R. Kumar, K. J. Arnold, S. J. Masson, A. S. Parkins, and M. D. Barrett, "Nonequilibrium phase transition in a spin-1 Dicke model," Optica **4**, 424 (2017).

[12] D. Nagy, G. Kónya, G. Szirmai, and P. Domokos, "Dicke-Model Phase Transition in the Quantum Motion of a Bose-Einstein Condensate in an Optical Cavity," Phys. Rev. Lett. **104**, 130401 (2010).

[13] K. Baumann, C. Guerlin, F. Brennecke, and T. Esslinger, "Dicke quantum phase transition with a superfluid gas in an optical cavity," Nature **464**, 1301 (2010).

[14] J. Léonard, A. Morales, P. Zupancic, T. Esslinger, and T. Donner, "Supersolid formation in a quantum gas breaking a continuous translational symmetry," Nature **543**, 87 (2017).

[15] R. Landig, L. Hruby, N. Dogra, M. Landini, R. Mottl, T. Donner, and T. Esslinger, "Quantum phases from competing short- and long-range interactions in an optical lattice," Nature **532**, 476 (2016).

[16] J. Klinder, H. Keßler, M. R. Bakhtiari, M. Thorwart, and A. Hemmerich, "Observation of a Superradiant Mott Insulator in the Dicke-Hubbard Model," Phys. Rev. Lett. **115**, 230403 (2015).

[17] A. J. Kollár, A. T. Papageorge, V. D. Vaidya, Y. Guo, J. Keeling, and B. L. Lev, "Supermode-density-wave-polariton condensation with a Bose-Einstein condensate in a multimode cavity," Nat. Commun. **8**, 14386 (2017).

[18] F. Mivehvar, F. Piazza, and H. Ritsch, "Disorder-Driven Density and Spin Self-Ordering of a Bose-Einstein Condensate in a Cavity," Phys. Rev. Lett. **119**, 063602 (2017).

[19] R. M. Kroeze, Y. Guo, V. D. Vaidya, J. Keeling, and B. L. Lev, "Spinor Self-Ordering of a Quantum Gas in a Cavity," Phys. Rev. Lett. **121**, 163601 (2018).

[20] F. Mivehvar, H. Ritsch, and F. Piazza, "A cavity-QED toolbox for quantum magnetism," (2018), 1809.09129.

[21] P. Domokos and H. Ritsch, "Collective Cooling and Self-Organization of Atoms in a Cavity," Phys. Rev. Lett. **89**, 253003 (2002).

[22] K. Baumann, R. Mottl, F. Brennecke, and T. Esslinger, "Exploring symmetry breaking at the dicke quantum phase transition," Phys. Rev. Lett. **107**, 140402 (2011).

[23] V. D. Vaidya, Y. Guo, R. M. Kroeze, K. E. Ballantine, A. J. Kollár, J. Keeling, and B. L. Lev, "Tunable-Range, Photon-Mediated Atomic Interactions in Multimode Cavity QED," Phys. Rev. X **8**, 011002 (2018).

[24] S. Gopalakrishnan, B. L. Lev, and P. M. Goldbart, "Emergent crystallinity and frustration with Bose-Einstein condensates in multimode cavities," Nat. Phys. **5**, 845 (2009).

[25] S. Gopalakrishnan, B. L. Lev, and P. M. Goldbart, "Atom-light crystallization of Bose-Einstein condensates in multimode cavities: Nonequilibrium classical and quantum Phase Transitions, emergent lattices, supersolidity, and frustration," Phys. Rev. A **82**, 043612 (2010).

[26] D. E. Chang, J. I. Cirac, and H. J. Kimble, "Self-Organization of Atoms along a Nanophotonic Waveguide," Phys. Rev. Lett. **110**, 113606 (2013).

[27] D. Porras and J. I. Cirac, "Effective quantum spin systems with trapped ions." Phys. Rev. Lett. **92**, 207901 (2004).
[28] K. Kim, M. S. Chang, R. Islam, S. Korenblit, L. M. Duan, and C. Monroe, "Entanglement and Tunable Spin-Spin Couplings between Trapped Ions Using Multiple Transverse Modes," Phys. Rev. Lett. **103**, 120502 (2009).
[29] J. W. Britton, B. C. Sawyer, A. C. Keith, C.-C. J. Wang, J. K. Freericks, H. Uys, M. J. Biercuk, and J. J. Bollinger, "Engineered two-dimensional Ising interactions in a trapped-ion quantum simulator with hundreds of spins," Nature **484**, 489 (2012).
[30] K. Kim, M.-S. Chang, S. Korenblit, R. Islam, E. E. Edwards, J. K. Freericks, G.-D. Lin, L.-M. Duan, and C. Monroe, "Quantum simulation of frustrated Ising spins with trapped ions," Nature **465**, 590 (2010).
[31] S. Gopalakrishnan, B. L. Lev, and P. M. Goldbart, "Frustration and Glassiness in Spin Models with Cavity-Mediated Interactions," Phys. Rev. Lett. **107**, 277201 (2011).
[32] P. Strack and S. Sachdev, "Dicke Quantum Spin Glass of Atoms and Photons," Phys. Rev. Lett. **107**, 277202 (2011).
[33] J. S. Douglas, H. Habibian, C. L. Hung, A. V. Gorshkov, H. J. Kimble, and D. E. Chang, "Quantum many-body models with cold atoms coupled to photonic crystals," Nature Photon **9**, 326 (2015).
[34] K. H. Fischer and J. A. Hertz, *Spin Glasses* (Cambridge University Press, Cambridge, 1991).
[35] D. L. Stein and C. M. Newman, *Spin Glasses and Complexity*, Primers in Complex Systems (Princeton University Press, 2013).
[36] A. E. Siegman, *Lasers* (University Science Books, 1986).
[37] L. G. Gouy, "Sur une propriété nouvelle des ondes lumineuse," C. R. Acad. Sci. Paris **110**, 1251 (1890); "Sur la propagation anomale des ondes," Ann. de Chim. et Phys. **24**, 145 (1891).
[38] R. W. Boyd, "Intuitive explanation of the phase anomaly of focused light beams," J. Opt. Soc. Am., JOSA **70**, 877 (1980).
[39] S. Feng and H. G. Winful, "Physical origin of the Gouy phase shift," Opt. Lett. **26**, 485 (2001).
[40] M. Padgett, "On the focussing of light, as limited by the uncertainty principle," J. Mod. Opt. **55**, 3083 (2008).
[41] T. D. Visser and E. Wolf, "The origin of the Gouy phase anomaly and its generalization to astigmatic wavefields," Optics Communications **283**, 3371 (2010).
[42] Reference [23] derived the nonlocal term under conditions of a traveling-wave pump. This work and Ref. [1] consider a standing-wave pump because this is likely to be used in the future to implement Ising spin models.
[43] This is true close to the center of the cavity and when we fix the longitudinal pattern of the TEM_{00} employed to be $\cos k_r z$ [1].
[44] This expansion is valid under the experimentally satisfied condition of low momentum excitation.
[45] See Supplemental Material [url] for information on experimental details and the effective Hamiltonian, which includes Ref. [56].
[46] A. J. Kollár, A. T. Papageorge, K. Baumann, M. A. Armen, and B. L. Lev, "An adjustable-length cavity and Bose-Einstein condensate apparatus for multimode cavity QED," New J. Phys. **17**, 43012 (2015).
[47] N. Schine, M. Chalupnik, T. Can, A. Gromov, and J. Simon, "Electromagnetic and gravitational responses of photonic Landau levels," Nature **565**, 173 (2019).
[48] The phase δ can be detected with a temporal heterodyne measurement [9, 13, 17].
[49] Finite-size effects likely bias the symmetry-breaking a small amount [22].
[50] We cannot determine the value of χ, only the relative phase shift.
[51] M. Endres, H. Bernien, A. Keesling, H. Levine, E. R. Anschuetz, A. Krajenbrink, C. Senko, V. Vuletić, M. Greiner, and M. D. Lukin, "Atom-by-atom assembly of defect-free one-dimensional cold atom arrays," Science **354**, 1024 (2016).
[52] D. Barredo, S. de Léséleuc, V. Lienhard, T. Lahaye, and A. Browaeys, "An atom-by-atom assembler of defect-free arbitrary two-dimensional atomic arrays," Science **354**, 1021 (2016).
[53] S. Gopalakrishnan, B. L. Lev, and P. M. Goldbart, "Exploring models of associative memory via cavity quantum electrodynamics," Philos. Mag. **92**, 353 (2012).
[54] V. Torggler, S. Krämer, and H. Ritsch, "Quantum annealing with ultracold atoms in a multimode optical resonator," Phys. Rev. A **95**, 032310 (2017).
[55] P. Rotondo, M. Marcuzzi, J. P. Garrahan, I. Lesanovsky, and M. Müller, "Open quantum generalisation of Hopfield neural networks," J. Phys. A **51**, 115301 (2018).
[56] K. Henderson, C. Ryu, C. MacCormick, and M. G. Boshier, "Experimental demonstration of painting arbitrary and dynamic potentials for Bose-Einstein condensates," New J. Phys. **11**, 043030 (2009).